

ExoMol molecular line lists: IX The spectrum of AlO

Andrei T. Patrascu, Sergei N. Yurchenko and Jonathan Tennyson
Department of Physics and Astronomy, University College London, London WC1E 6BT, UK

Accepted XXXX. Received XXXX; in original form XXXX

ABSTRACT

Accurate line lists are calculated for aluminium monoxide covering the pure rotation, rotation-vibration and electronic (B – X blue-green and A – X infrared bands) spectrum. Line lists are presented for the main isotopologue, $^{27}\text{Al}^{16}\text{O}$, as well as for $^{27}\text{Al}^{17}\text{O}$, $^{27}\text{Al}^{18}\text{O}$ and $^{26}\text{Al}^{16}\text{O}$. These line lists are suitable for high temperatures (up to 8000 K) including those relevant to exoplanetary atmospheres and cool stars. A combination of empirical and *ab initio* methods is used: the potential energy curves were previously determined to high accuracy by fitting to extensive data from analysis of laboratory spectra; a high quality *ab initio* dipole moment curve is calculated using quadruple zeta basis set and the multi-reference configuration interaction (MRCI) method. Partition functions plus full line lists of transitions are made available in an electronic form as supplementary data to this article and at www.exomol.com.

Key words: molecular data; opacity; astronomical data bases: miscellaneous; planets and satellites: atmospheres; stars: low-mass

1 INTRODUCTION

Aluminium monoxide (AlO) is an interesting astronomical species whose spectrum is prominent in a new class of Nova-stars first discovered by Tenenbaum & Ziurys (2009) of which the most prominent examples are probably V838 Mon and V4332 Sgr (Merrill et al. 1962; Bernard & Gravina 1984; Banerjee et al. 2005; Tylenda et al. 2005; Banerjee et al. 2012). These two objects defined a new type of eruptive variables called intermediate luminosity red transients and the observational data showed the intense presence of the near-infrared A – X system of the AlO radical. Indeed this A – X band is also found to be fairly prominent in a variety of cool, oxygen rich stars (Bernard & Gravina 1984; Banerjee et al. 2012): besides the Mira variables discussed above AlO emissions were also observed in the OH/IR stars and two bright infrared sources (Banerjee et al. 2012).

Transitions in the blue-green B – X system have been observed in sunspots (Sriramachandran et al. 2013) and the red supergiant VY Canis Majoris (Kaminski et al. 2013), in which millimeter-wave rotational transitions have also been observed (Tenenbaum & Ziurys 2009). Finally, AlO spectra have been used to try and determine abundance of the long-lived, radioactive ^{26}Al isotope (Banerjee et al. 2004).

Terrestrially AlO emissions arise from rocket exhausts in the atmosphere (Johnson 1965; Knecht et al. 1996). Its spectrum is also extensively used in the laboratory to monitor AlO in plasmas and other applications (Bescos et al. 1995; Naulin & Costes 1999; Glumac et al.

2001; Zhang & Li 2003; Bai et al. 2014; Surmick & Parigger 2014).

These applications, combined with technological uses of AlO spectra, have motivated a number of laboratory studies which have produced molecular constants characterising the lowest three states of AlO $X^2\Sigma^+$, $A^2\Pi$ and $B^2\Sigma^+$. There have also been attempts to produce line lists. Parigger & Hornkohl (2011) constructed a comprehensive line list for the X – B system for temperatures up to 6000 K but did not provide a transition dipole, so all their transition intensities are only relative. Launila & Berg (2011) performed a combined analysis of the A – X and B – X band systems involving 21 500 lines; we compare with some of their results below. There is, however, no single line list that combines a comprehensive set of transition frequencies with an accurate model for the transition intensities. It is this that we aim to do here as part of the ExoMol project. ExoMol aims to provide line lists of spectroscopic transitions for key molecular species which are likely to be important in the atmospheres of extrasolar planets and cool stars; its aims, scope and methodology have been summarised by Tennyson & Yurchenko (2012). Line lists for $^2\Sigma^+$ XH molecules, X = Be, Mg, Ca, have already been published (Yadin et al. 2012), as well as for a number of closed-shell diatomics (Barton et al. 2013, 2014; Yorke et al. 2014). In the present paper, we present rotation-vibration transition lists and associated spectra for AlO. These line lists are particularly comprehensive and should be valid for temperatures up to 8000 K.

2 METHOD

Rotation-vibration line lists for the three lower electronic states of AIO were obtained by direct solution of the nuclear motion Schrödinger equation using program DUO (Yurchenko et al. 2015). The calculations require both a potential energy curve (PEC) for each of the three states considered and also couplings between these curves. These curves were taken from our previous study (Patrascu et al. 2014), which computed *ab initio* potential energies, spin-orbit and electronic angular momenta couplings, and refined them using available experimental data. Nuclear motion calculations using these refined curves showed that the observed transition frequencies and energy levels could be reproduced with root mean square error of only 0.07 cm^{-1} . In order to cover all vibrational excitations below $35,000 \text{ cm}^{-1}$, we have increased the sizes of the vibrational basis set to 90 for each of the X, A, and B states from those used by Patrascu et al. (2014). The ranges of rotational excitations are listed in Table 2.

2.1 Dipole moments

There appears to be no experimental measurements of any AIO transition dipoles. For this reason we constructed new dipole moment curves (DMC) using high level *ab initio* calculations. These are compared to previous, high-level *ab initio* determinations (Zenouda et al. 1999) below. The *ab initio* calculations were performed using MOLPRO (Werner et al. 2010); we used multi-reference configuration interaction (MRCI) methods with different choices of basis sets. Our optimal basis choice was aug-cc-pVQZ; the active space used in MOLPRO representation was (9,4,4). Electronic dipole moments as function of bondlength, R , were computed as the expectation value

$$\mu(R) = e \langle \Psi_M | \sum_i \underline{r}_i | \Psi_N \rangle, \quad (1)$$

where the integral and the summation run over the electron coordinates, denoted by \underline{r}_i , and e is the charge of the electron. For permanent dipole moments, the electronic wavefunctions in the bra and ket are the same, ie $M = N$, and the dipole moment, which is denoted $\mu(M)$ below, also contains a term due to permanent nuclear charge. For transition dipole moments, $M \neq N$, and the dipole is denoted is $\mu(M - N)$ below. For transition dipole moments, care must be taken to ensure that the dipole phases are consistent as a function of R (Tennyson 2014; Patrascu et al. 2014).

Our calculations produce the values for the dipole at equilibrium given in Table 1 which compare well to the previous results obtained by Zenouda et al. (1999). Our ground state value of the dipole and that of Zenouda et al. (1999) are both slightly smaller than the value 4.60 D used in the JPL database (Pickett et al. 1998) which was taken from the earlier calculations of Lingsfield & Liu (1982).

Figures 1 and 2 compare our calculated diagonal and off-diagonal DMCs, respectively, with those of Zenouda et al. (1999). The agreement is good. Our calculations suggest that the $\mu(\text{B-A})$ DMC is small at all geometries meaning that the B – A band will be very weak; a similar conclusion was reached by Partridge et al. (1983).

Table 1. *Ab initio* electric dipole and transition dipole moments in Debye at $R = 1.76 \text{ \AA}$.

Transition moments	This Work	Zenouda et al. (1999) ^a
X $^2\Sigma^+$	−4.39	−4.24
A $^2\Pi$	−1.30	−1.40
B $^2\Sigma^+$	−2.18	−2.27
X $^2\Sigma^+ - \text{B } ^2\Sigma^+$	1.85	1.66
X $^2\Sigma^+ - \text{A } ^2\Pi$	0.61	0.61
B $^2\Sigma^+ - \text{A } ^2\Pi$	−0.046	

^a The signs of the diagonal dipoles have been changed to conform to the convention used by MOLPRO.

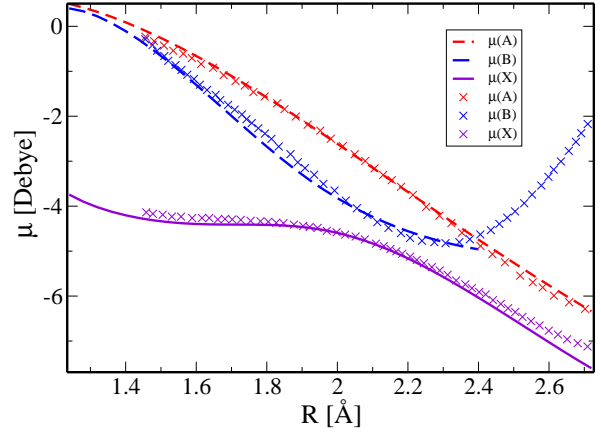


Figure 1. *Ab initio* permanent dipole moment curves for AIO for the lowest three electronic states. The previous calculations by Zenouda et al. (1999) are represented by crosses.

The *ab initio* DMC grid points were used directly in DUO to produce a line list for AIO.

There is a lack of experimental data on AIO transition dipoles or transition intensities. Table 2 therefore compares the lifetime for the $\text{B } ^2\Sigma^+$ state with experimental data available from Johnson et al. (1972); Dagdigian et al. (1975) and two *ab initio* estimates from Partridge et al. (1983). For Partridge et al. (1983) we have taken their figures which include the small contribution from the weak B – A decay channel since this contribution is also included in our estimate. Our lifetimes were computed by summing over all decays from a given $\text{B } ^2\Sigma^+ (v, J)$. Our results in Table 2 are for $J = 0.5$; calculations for $J = 24.5$, which lies in the region of the band head, give lifetimes about 0.5 % longer. We conclude that the lifetimes are not strongly J -dependent. In common with the other studies we find that the lifetime grows slowly with v . Our results are intermediate between the two predictions of Partridge et al. (1983) and slightly shorter than, but marginally consistent with, the measurements of Dagdigian et al. (1975). The measurements of Johnson et al. (1972) give longer lifetimes than all studies and we suggest these are too long.

Table 2. Radiative lifetimes (nsec) for B²Σ⁺ state of AlO, compared to the measurements of Johnson et al. (1972) and Dagdigian et al. (1975), and the two separate calculations of Partridge et al. (1983).

Vibrational Level	This work	Partridge et al. (1983) I	Partridge et al. (1983) II	Johnson et al. (1972)	Dagdigian et al. (1975)
0	92.4	88.1	109.9	128 ± 6	100 ± 7
1	94.5	90.5	112.6	125 ± 3	102 ± 7
2	96.7	93.0	115.2	130 ± 7	102 ± 4

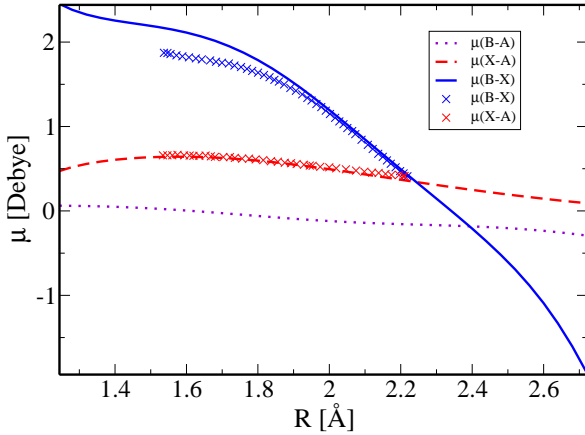


Figure 2. *Ab initio* transition dipole moment curves for AlO linking the lowest three electronic states. The previous calculations by Zenouda et al. (1999) are represented by crosses.

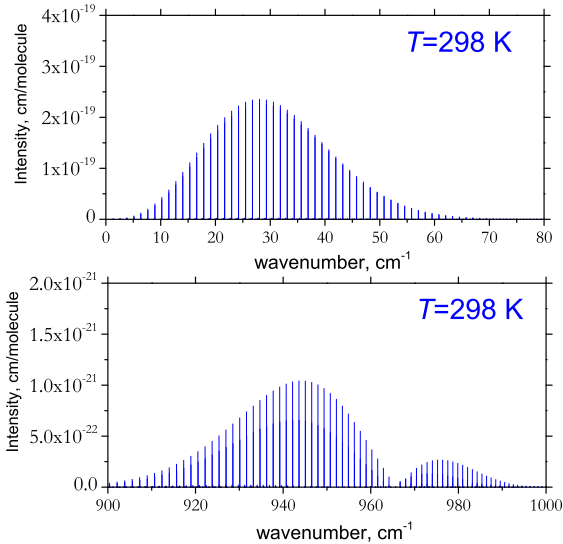


Figure 3. Computed spectra of ²⁷Al¹⁶O at T=298 K given as sticks with the intensity (cm molecule⁻¹) represented by their height. Upper panel: rotational region; lower panel: vibrational fundamental.

2.2 Partition function

Partition functions for AlO were calculated by summing all the calculated energy levels below using DUO (Yurchenko et al. 2015). When summing these levels it is necessary to multiply by the appropriate degeneracy factors. Since we follow HITRAN (Fischer et al. 2003) and use the full nuclear spin degeneracy, the degeneracy factor, g , is given by $(2J + 1)(2I_{Al} + 1)(2I_O + 1)$ where J is the total angular momentum quantum number obtained by adding the rotational and spin angular momenta. I_{Al} and I_O are the nuclear spins of the isotopes of Al and O in the given isotopologue. Explicit inclusion of these nuclear spin factors accounts for hyperfine effects which we make no attempt to resolve. These factors are 11, 6, 1, 6 and 1 for ²⁶Al, ²⁷Al, ¹⁶O, ¹⁷O and ¹⁸O, respectively.

Table 3 compares our results for ²⁷Al¹⁶O with those of Sauval & Tatum (1984). We have multiplied the results of Sauval & Tatum (1984) by the appropriate nuclear spin factors to bring their results into line with our convention outlined above. Table 3 shows good agreement between our ²⁷Al¹⁶O partition function and that given by (Sauval & Tatum 1984) at temperatures above 1000 K for which their results are valid. At lower temperatures we also agree well with the partition function given by JPL (Pickett et al. 1998) who, for example, give $Q(300) = 3926.45$ which is slightly lower than our value of 3966.90, probably due to neglect of the contribution of excited vibrational states.

As we use all ro-vibrational energy levels there are no issues with convergence of this sum. We follow Vidler & Tennyson (2000) and represent our partition function using the following functional form

$$\log_{10} Q(T) = \sum_{n=0}^8 a_n [\log_{10} T]^n \quad (2)$$

where the fitting parameters a_n are given in Table 4. These fits reproduce the partition functions for the entire region below 9000 K with a relative root-mean-square (rms) errors of better than 1.6 %.

2.3 Line list calculations

Line lists were calculated for the four isotopologues ²⁷Al¹⁶O, ²⁷Al¹⁸O, ²⁷Al¹⁷O, and ²⁶Al¹⁶O. All rotation-vibration states were considered and transitions satisfying the dipole selection rule $\Delta J = 0, \pm 1$. These line lists span frequencies up to 35 000 cm⁻¹ ($\lambda > 0.286 \mu\text{m}$). The procedure described above was used to produce line lists, i.e. catalogues of transition frequencies $\tilde{\nu}_{ij}$ and Einstein coefficients A_{ij} , for four Aluminium oxide isotopologues ²⁷Al¹⁶O, ²⁷Al¹⁸O, ²⁷Al¹⁷O,

Table 4. Partition function parameters for various isotopologues, see Eq. (2)

	$^{27}\text{Al}^{16}\text{O}$	$^{27}\text{Al}^{18}\text{O}$	$^{26}\text{Al}^{16}\text{O}$	$^{27}\text{Al}^{17}\text{O}$
a_0	-1.04093681038	-1.59727184392	-0.677569296333	-0.541673874468
a_1	9.64080670554	11.9848644854	9.21909668136	10.8157290731
a_2	-14.3512337912	-18.2945471026	-13.6457740234	-16.3230021925
a_3	13.0627960677	16.7055086746	12.4154930773	14.8789580623
a_4	-7.20103828655	-9.21814194734	-6.84559240132	-8.20306751046
a_5	2.49431683028	3.17902318889	2.37492955521	2.83289571369
a_6	-0.538890191754	-0.677958762340	-0.514966111414	-0.607255974396
a_7	0.0673568508718	0.0828183310157	0.0647424233238	0.0749009373167
a_8	-0.00372906050126	-0.004450320873	-0.00360977781061	-0.00407761291349

Table 5. Summary of our AIO line lists.

	$^{27}\text{Al}^{16}\text{O}$	$^{27}\text{Al}^{18}\text{O}$	$^{26}\text{Al}^{16}\text{O}$	$^{27}\text{Al}^{17}\text{O}$
X $^2\Sigma^+$				
Maximum v	66	69	66	68
Maximum J	300.5	300.5	300.5	300.5
A $^2\Pi$				
Maximum v	63	65	62	64
Maximum J	300.5	300.5	300.5	300.5
B $^2\Sigma^+$				
Maximum v	40	41	39	40
Maximum J	232.5	241.5	230.5	237.5
Number of lines	4 945 580	5 365 592	4 866 540	5 148 996

Table 3. Partition function, $Q(T)$, for $^{27}\text{Al}^{16}\text{O}$, as a function of temperature.

T / K	Q(T)	T	Q(T)	Sauval & Tatum (1984)
10	134.73	1000	17595.69	17693.4
20	265.35	2000	57302.56	57060.6
30	396.01	3000	138649.47	135168
40	526.68	4000	283031.72	274740
50	657.37	5000	508066.61	487708
60	788.07	6000	828224.93	793980
70	918.78	7000	1254881.70	1216536
80	1049.50	8000	1795616.84	1781718
100	1310.96			
200	2621.45			
300	3966.90			
400	5407.40			
500	6988.27			
600	8734.58			
750	11692.87			

and $^{26}\text{Al}^{16}\text{O}$. The full line list for each of the studied isotopologues are summarised in Table 5.

3 RESULTS

The line lists contain about 5 million transitions each and, therefore, for compactness and ease of use, are divided into separate energy level and transitions file. This is done using standard ExoMol format (Tennyson et al. 2013) which is based on a method originally developed for the BT2 line list (Barber et al. 2006). Extracts for the start of the $^{26}\text{Al}^{16}\text{O}$ files are given in Tables 6 and 7. The full line list for each of

these isotopologues can be downloaded from the CDS, via <ftp://cdsarc.u-strasbg.fr/pub/cats/J/MNRAS/xxx/yy>, or <http://cdsarc.u-strasbg.fr/viz-bin/qcat?J/MNRAS//xxx/yy>.

The line lists and partition function together with auxiliary data including the potential parameters and dipole moment functions, as well as the absorption spectrum given in cross section format (Hill et al. 2013), can all be obtained from there as well as at www.exomol.com.

Figure 3 shows the rotational component, and the P- and weaker R-branches of the vibrational fundamental ($v = 0 - 1$) obtained at $T=298$ K. As has been noted before (Lengsfeld & Liu 1982), the X-state dipole is very flat in the equilibrium region. As the strength of a $\Delta v = 1$ vibration-rotation transition depends on the slope of the dipole in this region, this causes the vibrational fundamental to be particularly weak. Therefore this feature, which lies between 10 and 11 μm , is unlikely to be astronomically important. Our calculations suggest that the overtones ($\Delta v > 1$) are also weak so the entire AIO vibration-rotation spectrum is unlikely to feature strongly in astronomical objects.

Much more significant at infrared wavelengths is the A – X electronic band. Figure 4 shows an overview of the A – X and B – X electronic transitions which are presented as absorption spectra generated at $T = 2000$ K. Our spectra are compared to available experimental data (Launila & Jonsson 1994; Saksena et al. 2008): we note that these measurements do not give absolute intensities, so have been scaled by us. A more detailed comparison of a portion of the A – X spectrum with the experimental results of Launila & Berg (2011) is presented in Fig. 5. Figure 6 compares the theoretical spectrum obtained here with an astronomical spectrum of Kaminski et al. (2013). The agreement is remarkable. The calculation performed using the vi-

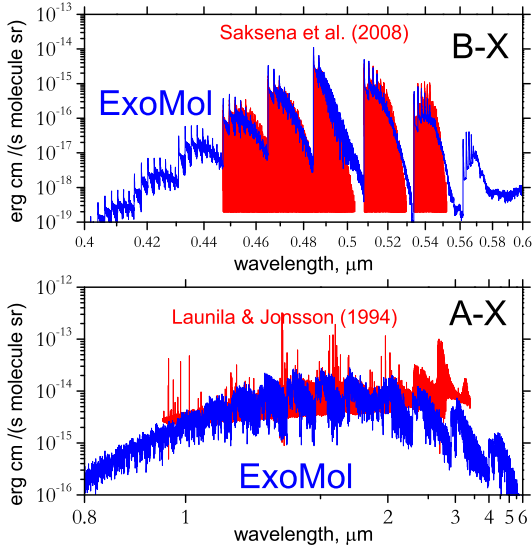


Figure 4. Overview of the theoretical (ExoMol) and experimental (Launila & Jonsson 1994; Saksena et al. 2008) spectra of $^{27}\text{Al}^{16}\text{O}$. The theoretical spectra were obtained as cross sections convolved with a Gaussian line profile of width 1 cm^{-1} assuming the local thermal equilibrium at $T = 2000\text{ K}$. The experimental A – X and B – X spectra were scaled by 1×10^{-17} and 5×10^{-18} , respectively.

brational T_{vib} and rotational T_{rot} temperatures of 2200 K and 700 K , respectively as suggested by Kaminski et al. (2013). We use a gaussian convolution with the half-width at half-maximum derived of 0.3 cm^{-1} to match the spectrum by Kaminski et al. (2013). Also shown (in red) is the simulation of their observed spectrum by Kaminski et al. (2013); for this they generated their own line list based on the line positions of Saksena et al. (2008), transition moments of Zenouda et al. (1999), Franck-Condon factors of Coxon & Naxakis (1985) and rotational line-strength factors which they computed themselves. We note that our line list provides all these data within a single framework and without making any underlying assumptions about the Franck-Condon approximation or rotational form factors.

Figure 7 compares the B – X emission spectrum obtained in this work with accurate experimental results of Saksena et al. (2008). Again the agreement is very good. Finally, Fig. 8 compares our calculated spectra B – X for the two isotopologues $^{26}\text{Al}^{16}\text{O}$ and $^{27}\text{Al}^{16}\text{O}$. The shift in the band head feature should be observable astronomically at even moderate resolution.

4 CONCLUSIONS

We present comprehensive line lists for the four most important isotopologues of AlO. These are based on the direct solution of the nuclear motion Schrödinger equation using a potential energy curves and couplings obtained by fitting to extensive dataset of measured transitions. These data are reproduced to near experimental accuracy resulting in high

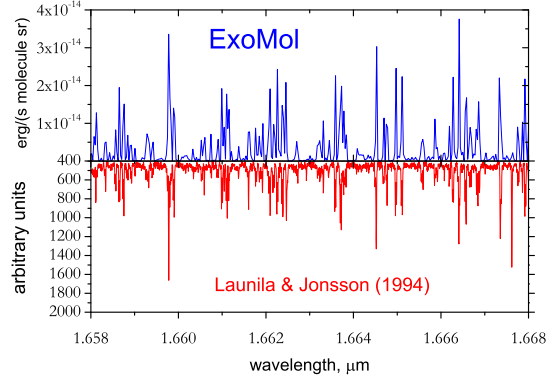


Figure 5. A – X emission spectrum of $^{27}\text{Al}^{16}\text{O}$, comparison with experiments of Launila & Jonsson (1994) at $T = 3200\text{ K}$. The theoretical spectrum was obtained as cross sections convolved with a Doppler line profile assuming the local thermal equilibrium at $T = 3200\text{ K}$.

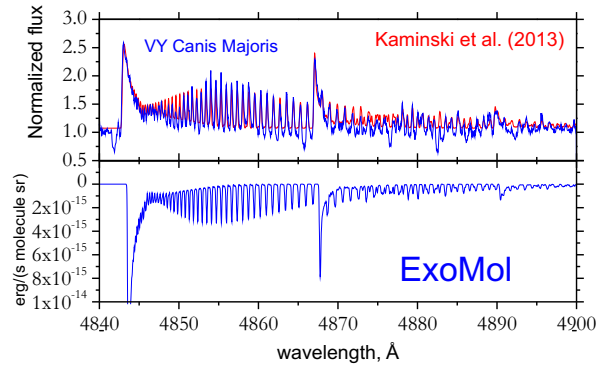


Figure 6. B – X $\Delta v = 0$ emission spectrum at $T_{\text{rot}} = 700\text{ K}$ and $T_{\text{vib}} = 2200\text{ K}$ compared with an astronomical spectrum obtained by Kaminski et al. (2013) for VY Canis Majoris (T_{rot} and T_{vib} in (Kaminski et al. 2013)). Cross sections (lower part) were obtained by convolving with a Gaussian profile of width 0.3 cm^{-1} .

accuracy line positions. A new *ab initio* dipole moment is computed. This dipole is used to compute Einstein A coefficients for all possible dipole-allowed transitions within each AlO isotopologue. The result is a comprehensive line list for each species. The line lists can be downloaded from the CDS, via <ftp://cdsarc.u-strasbg.fr/pub/cats/J/MNRAS/>, or <http://cdsarc.u-strasbg.fr/viz-bin/qcat?J/MNRAS/>, or from www.exomol.com.

ACKNOWLEDGEMENTS

This work is supported by ERC Advanced Investigator Project 267219.

REFERENCES

- Bai X., Motto-Ros V., Lei W., Zheng L., Yu J., 2014, *Spectra Chimica Acta B*, 99, 193

Table 6. Extract from the state file for $^{27}\text{Al}^{16}\text{O}$. Full tables are available from <http://cdsarc.u-strasbg.fr/cgi-bin/VizieR?-source=J/MNRAS/xxx/yy>.

n	E	g	J	$+/-$	e/f	State	v	$ \Lambda $	$ \Sigma $	$ \Omega $
1	0.000000	12	0.5	+	e	X2SIGMA+	0	0	0.5	0.5
2	965.435497	12	0.5	+	e	X2SIGMA+	1	0	0.5	0.5
3	1916.845371	12	0.5	+	e	X2SIGMA+	2	0	0.5	0.5
4	2854.206196	12	0.5	+	e	X2SIGMA+	3	0	0.5	0.5
5	3777.503929	12	0.5	+	e	X2SIGMA+	4	0	0.5	0.5
6	4686.660386	12	0.5	+	e	X2SIGMA+	5	0	0.5	0.5
7	5346.116382	12	0.5	+	e	A2PI	0	1	0.5	0.5
8	5581.906844	12	0.5	+	e	X2SIGMA+	6	0	0.5	0.5
9	6066.934830	12	0.5	+	e	A2PI	1	1	0.5	0.5
10	6463.039443	12	0.5	+	e	X2SIGMA+	7	0	0.5	0.5
11	6778.997803	12	0.5	+	e	A2PI	2	1	0.5	0.5
12	7329.427637	12	0.5	+	e	X2SIGMA+	8	0	0.5	0.5
13	7483.145675	12	0.5	+	e	A2PI	3	1	0.5	0.5
14	8159.170405	12	0.5	+	e	A2PI	4	1	0.5	0.5
15	8201.467744	12	0.5	+	e	X2SIGMA+	9	0	0.5	0.5
16	8857.266385	12	0.5	+	e	A2PI	5	1	0.5	0.5
17	9029.150380	12	0.5	+	e	X2SIGMA+	10	0	0.5	0.5
18	9535.195842	12	0.5	+	e	A2PI	6	1	0.5	0.5
19	9854.882567	12	0.5	+	e	X2SIGMA+	11	0	0.5	0.5
20	10204.019475	12	0.5	+	e	A2PI	7	1	0.5	0.5
21	10667.668381	12	0.5	+	e	X2SIGMA+	12	0	0.5	0.5
22	10864.560220	12	0.5	+	e	A2PI	8	1	0.5	0.5
23	11464.897083	12	0.5	+	e	X2SIGMA+	13	0	0.5	0.5
24	11519.212123	12	0.5	+	e	A2PI	9	1	0.5	0.5
25	12156.974798	12	0.5	+	e	A2PI	10	1	0.5	0.5
26	12257.694655	12	0.5	+	e	X2SIGMA+	14	0	0.5	0.5
27	12793.671660	12	0.5	+	e	A2PI	11	1	0.5	0.5
28	13030.412255	12	0.5	+	e	X2SIGMA+	15	0	0.5	0.5
29	13421.583651	12	0.5	+	e	A2PI	12	1	0.5	0.5
30	13790.933964	12	0.5	+	e	X2SIGMA+	16	0	0.5	0.5

 n : State counting number. \tilde{E} : State energy in cm^{-1} . J : Total angular momentum quantum number. g : State degeneracy. $+/-$: Total parity. e/f : Rotationless-parity (Brown et al. 1975). v : State vibrational quantum number. $|\Lambda|$: Absolute value of Λ (projection of the electronic angular momentum). $|\Sigma|$: Absolute value of Σ (projection of the electronic spin). $|\Omega|$: Absolute value of $\Omega = \Lambda + \Sigma$ (projection of the total angular momentum).

Banerjee D. P. K., Ashok N. M., Launila O., Davis C. J., Varricatt W. P., 2004, *ApJ*, 610, L29
Banerjee D. P. K., Barber R. J., Ashok N. K., Tennyson J., 2005, *ApJ*, 627, L141
Banerjee D. P. K., Varricatt W. P., Mathew B., Launila O., Ashok N. M., 2012, *Astrophys. J. Lett.*, 753, L20
Barber R. J., Tennyson J., Harris G. J., Tolchenov R. N., 2006, *MNRAS*, 368, 1087
Barton E. J., Chiu C., Golpayegani S., Yurchenko S. N., Tennyson J., Frohman D. J., Bernath P. F., 2014, *MNRAS*, 442, 1821
Barton E. J., Yurchenko S. N., Tennyson J., 2013, *MNRAS*, 434, 1469
Bernard A., Gravina R., 1984, *Z. Naturforsch. Sect. A-J. Phys. Sci.*, 39, 1049
Bescos B., Morley G., Urena A. G., 1995, *Chem. Phys. Lett.*, 244, 407
Brown J. M. et al., 1975, *J. Mol. Spectrosc.*, 55, 500
Coxon J. A., Naxakis S., 1985, *J. Mol. Spectrosc.*, 111, 102

Dagdigian P. J., Cruse H. W., Zare R. N., 1975, *J. Chem. Phys.*, 62, 1824
Fischer J., Gamache R. R., Goldman A., Rothman L. S., Perrin A., 2003, *J. Quant. Spectrosc. Radiat. Transf.*, 82, 401
Glumac N. G., Servaites J., Krier H., 2001, *Combust. Sci. Technol.*, 172, 97
Hill C., Yurchenko S. N., Tennyson J., 2013, *Icarus*, 226, 1673
Johnson E. R., 1965, *J. Geophys. Res.*, 70, 1275
Johnson S. E., Capelle G., Broida H. P., 1972, *J. Chem. Phys.*, 56, 663
Kaminski T., Schmidt M. R., Menten K. M., 2013, *A&A*, 549, A6
Knecht D. J., Pike C. P., Murad E., Rall D. L. A., 1996, *J. Spacecrafts Rockets*, 33, 677
Launila O., Berg L.-E., 2011, *J. Mol. Spectrosc.*, 265, 10
Launila O., Jonsson J., 1994, *J. Mol. Spectrosc.*, 168, 1
Lengsfeld B. H., Liu B., 1982, *J. Chem. Phys.*, 77, 6083

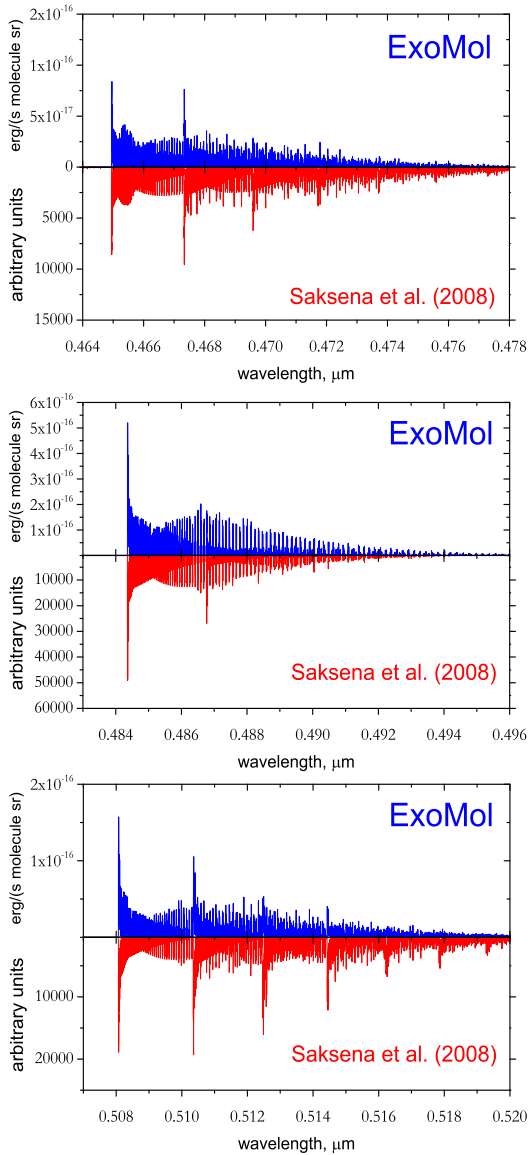


Figure 7. Emission spectra of three sub-bands within the X – B band at 1700 K compared to the experiment of Saksena et al. (2008) (up). Top panel: $\Delta v = 1$, middle panel: $\Delta v = 0$, lower panel: $\Delta v = -1$. The experimental data is in arbitrary units; calculated cross sections were obtained by convolving with a Doppler profile at 1700 K.

- Merrill P. W., Keenan P. C., Deutsch A. J., 1962, ApJ, 136, 21
 Naulin C., Costes M., 1999, Chem. Phys. Lett., 310, 231
 Parigger C. G., Hornkohl J. O., 2011, Spectra Chimica Acta A, 81, 404
 Partridge H., Langhoff S. R., Lengsfeld B. H., Liu B., 1983, J. Quant. Spectrosc. Radiat. Transf., 30, 449
 Patrascu A. T., Hill C., Tennyson J., Yurchenko S. N., 2014, J. Chem. Phys., 141, 144312
 Pickett H. M., Poynter R. L., Cohen E. A., Delitsky M. L., Pearson J. C., Müller H. S. P., 1998, J. Quant. Spectrosc. Radiat. Transf., 60, 883

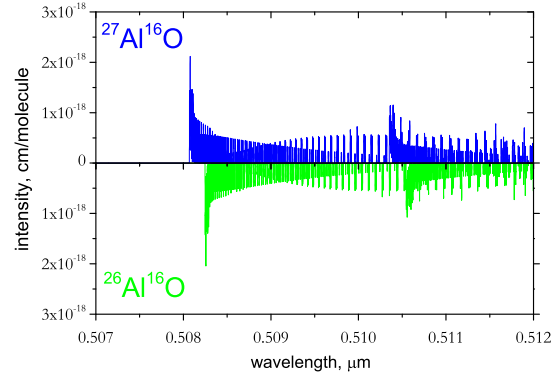


Figure 8. Calculated B – X $v' - v'' = 0 - 1$ absorption spectrum at 1700 K for $^{26}\text{Al}^{16}\text{O}$ and $^{27}\text{Al}^{16}\text{O}$ obtained by convolving with a Doppler profile at 1700 K.

Table 7. Extracts from the transitions file for $^{27}\text{Al}^{16}\text{O}$. Full tables are available from <http://cdsarc.u-strasbg.fr/cgi-bin/VizieR?-source=J/MNRAS/xxx/yy>.

f	i	A_{fi}
47156	47355	$1.1598E - 04$
9373	8773	$5.0797E - 02$
10989	10389	$1.5734E - 02$
10789	10589	$1.5455E - 02$
9755	9155	$6.3206E - 03$
12788	13387	$2.7204E - 06$
10178	9578	$2.3282E - 02$
9555	9355	$6.7365E - 03$
9187	8987	$5.4996E - 02$
9587	9387	$5.4633E - 02$
7360	7159	$9.1545E - 06$
9184	9384	$4.8954E - 05$
9751	9151	$5.9125E - 03$
9551	9351	$5.9229E - 03$
10166	9566	$8.9220E - 03$
10985	10385	$1.4584E - 02$
10785	10585	$1.4584E - 02$
8548	7948	$5.1842E - 02$
20975	20775	$5.7037E - 05$
8148	7548	$5.2229E - 02$
9966	9766	$9.1712E - 03$

f : Upper state counting number; i : Lower state counting number; A_{fi} : Einstein-A coefficient in s^{-1} .

- Saksena M. D., Deo M. N., Sunanda K., Behere S. H., Londhe C. T., 2008, J. Mol. Spectrosc., 247, 47
 Sauval A. J., Tatum J. B., 1984, ApJS, 56, 193
 Sriramachandran P., Viswanathan B., Shanmugavel R., 2013, Sol. Phys., 286, 315
 Surmick D. M., Parigger C. G., 2014, Appl. Spectrosc., 68, 992
 Tenenbaum E. D., Ziurys L. M., 2009, ApJ, 694, L59
 Tennyson J., 2014, J. Mol. Spectrosc., 298, 1
 Tennyson J., Hill C., Yurchenko S. N., 2013, in AIP Conference Proceedings, Vol. 1545, 6th international conference on atomic and molecular data and their applications ICAMDATA-2012, AIP, New York, pp. 186–195
 Tennyson J., Yurchenko S. N., 2012, MNRAS, 425, 21

- Tylenda R., Crause L. A., Gorny S. K., Schmidt M. R.,
2005, *A&A*, 439, 651
- Vidler M., Tennyson J., 2000, *J. Chem. Phys.*, 113, 9766
- Werner H. J., Knowles P. J., Lindh R., Manby F. R., Schütz
M., 2010, MOLPRO, a package of ab initio programs. See
<http://www.molpro.net/>
- Yadin B., Vaness T., Conti P., Hill C., Yurchenko S. N.,
Tennyson J., 2012, *MNRAS*, 425, 34
- Yorke L., Yurchenko S. N., Lodi L., Tennyson J., 2014,
MNRAS, 445, 1383
- Yurchenko S. N., Lodi L., Tennyson J., Stolyarov A. V.,
2015, *Comput. Phys. Commun.*
- Zenouda C., Blottiau P., Chambaud G., Rosmus P., 1999,
J. Molec. Struct. (THEOCHEM), 458, 61
- Zhang S. D., Li H. Y., 2003, *Chem. Res. Chin. Univ.*, 19,
320

